

A Direct Algorithm for Ultrasound Imaging of Internal Corrosion*

Habib Ammari[†] Hyeonbae Kang[‡] Eunjoo Kim[§] Mikyoung Lim[¶]
Kaouthar Louati^{||}

Abstract

We develop a direct (non-iterative) algorithm to address the inverse problem of identifying a collection of disjoint internal corrosive parts of small Hausdorff measures in pipelines from exterior ultrasound boundary measurements. The method is based on an asymptotic expansion of the effect of the corrosion in terms of the size of the corrosive parts. We numerically test the validity of the asymptotic formula at high frequencies. We also propose a simple procedure to remove high-frequency instabilities in our inversion procedure. We illustrate our main findings with a variety of computational examples.

Mathematics subject classification (MSC2000): 35R30

Keywords: direct imaging, corrosion, asymptotic representation formula, reconstruction, ultrasound detection, high frequencies, MUSIC-type algorithm

1 Introduction

Corrosion detection remains a topic of considerable activity in the inverse problems community. Of special interest are algorithms that make use of a priori information or assumptions concerning the nature of target's internal structure. Such assumptions can usually be exploited to obtain much faster, simpler and more stable algorithms than would otherwise be possible.

In this paper we consider the problem of determining the corrosion damage of an inaccessible part of the surface of a specimen from ultrasound measurements.

The impedance imaging problem for detecting internal corrosion was considered in [7]. In that paper the authors propose an algorithm of MUSIC (multiple signal classification) type [3, 10, 12, 13] for detecting corrosive parts in pipelines from input fluxes. This algorithm

*This work was supported by the ANR, the KOSEF grant No. 2009-0070442, KRF-2008-359-C00004, KRF-2008-220-C00002, and NRF20090085987.

[†]Department of Mathematics and Applications, Ecole Normale Supérieure, 45 Rue d'Ulm, 75005 Paris, France (habib.ammari@ens.fr).

[‡]Department of Mathematics, Inha University, Incheon 402-751, Korea (hbkang@inha.ac.kr).

[§]Department of Mathematics, Ewha Womans University, Seoul 120-750, Korea (kim123ej@hanmail.net)

[¶]Department of Mathematical Sciences, Korean Advanced Institute of Science and Technology, 335 Gwahangno (373-1 Guseong-dong), Yuseong-gu, Daejeon 305-701, Korea (mklim@kaist.ac.kr).

^{||}Centre de Mathématiques Appliquées, Ecole Polytechnique, 91128 Palaiseau Cedex, France (louati@cmmapx.polytechnique.fr).

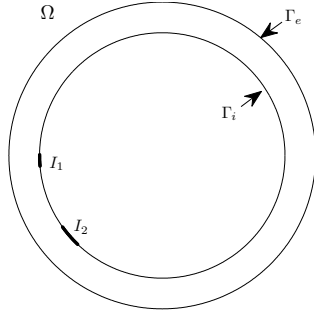


Figure 1: The geometry of the problem with $m = 2$.

is based on an accurate asymptotic representation formula for the steady state voltage perturbations.

In this paper, we adapt the MUSIC-type algorithm of [7] to the setting in which multiple ultrasound boundary measurements are available and also show how one may quantitatively deduce the number of corrosive parts present. Our approach relies on an asymptotic expansion of the ultrasound reflected wave with respect to the length of the corrosive parts. Yet another method for corrosion detection, the vibration testing, has been considered in a recent paper [5]. Preliminary versions of this paper's results have been compared with results by electrostatic and vibration testings [4]. The method of this paper (ultrasound measurements) seems to perform as good as that of electrostatic imaging, while the result by vibration testing seems to be the worst, which is natural because the modal measurements are limited.

The organization of the paper is as follows. In Section 2 we state the forward and corresponding inverse problem of interest, then review some basic facts on Green's functions. In Section 3 we state our main theorem that allows us in Section 4 to develop our MUSIC-type algorithm for recovering a collection of corrosive parts. High oscillations in the measurements data cause a challenging difficulty in inverse scattering problems [14, 15]. In Section 5 we briefly discuss how to resolve this difficulty in our case. In Section 6 we provide several computational examples, as well as concluding remarks. We consider only the two-dimensional case, the extension to three dimensions being obvious.

2 Preliminaries and formulation of the inverse problem

Let us first fix notation for this work. Let the annulus $\Omega = \{x : r < |x| < R\}$ represent the specimen to be inspected. Let Γ_e and Γ_i denote the circles of radius R and r centered at the origin, respectively. Suppose that the inaccessible surface Γ_i contains some corrosive parts I_s , $s = 1, \dots, m$. See Figure 1. The parts I_s are well-separated and the reciprocal of the surface impedance (the corrosion coefficient) of each I_s , $s = 1, \dots, m$, is $\gamma_s \geq 0$, not

identically zero. We assume that each $\gamma_s \in \mathcal{C}^1(I_s)$. Let

$$\gamma(x) = \sum_{s=1}^m \gamma_s(x) \chi_s(x), \quad x \in \Gamma_i, \quad (2.1)$$

where χ_s denotes the characteristic function of I_s . The annulus Ω in two dimensions may be considered as a cross section of a pipe inside which there are corrosive parts. We assume that the Hausdorff measures (length) of I_s are small:

$$|I_s| = O(\epsilon), \quad s = 1, \dots, m, \quad (2.2)$$

where ϵ is a small parameter representing the common order of magnitude of I_s . Here and throughout this paper $|\cdot|$ denotes the one dimensional Hausdorff measure. Then for each $p \geq 1$, we have

$$\|\gamma\|_{L^p(\Gamma_i)} \leq C\epsilon^{1/p}. \quad (2.3)$$

For $\omega > 0$, a fundamental solution $\Phi_\omega(x)$ to the Helmholtz operator $\Delta + \omega^2$ in \mathbb{R}^2 is given by

$$\Phi_\omega(x) = -\frac{i}{4} H_0^{(1)}(\omega|x|), \quad (2.4)$$

for $x \neq 0$, where $H_0^{(1)}$ is the Hankel function of the first kind of order 0. The ultrasound wave u_γ generated by a source at $y \in \Gamma_e$ satisfies

$$\begin{cases} (\Delta + \omega^2)u_\gamma = 0 & \text{in } \Omega, \\ \frac{\partial u_\gamma}{\partial \nu} + \gamma u_\gamma = 0 & \text{on } \Gamma_i, \\ u_\gamma = \Phi_\omega(\cdot - y) & \text{on } \Gamma_e, \end{cases} \quad (2.5)$$

where ν is the outward unit normal to Ω .

Let u_0 denote the solution in absence of the corrosion, *i.e.*, the solution to the problem

$$\begin{cases} (\Delta + \omega^2)u_0 = 0 & \text{in } \Omega, \\ \frac{\partial u_0}{\partial \nu} = 0 & \text{on } \Gamma_i, \\ u_0 = \Phi_\omega(\cdot - y) & \text{on } \Gamma_e. \end{cases} \quad (2.6)$$

Throughout this paper, we suppose that ω is not an eigenvalue of $-\Delta$ in Ω with the Dirichlet boundary condition on Γ_e and the Neumann boundary condition on Γ_i . Using the theory of collectively compact operators [2], we can easily prove that (2.5) is uniquely solvable for $\|\gamma\|_{L^p}$ small enough.

Define the Dirichlet function G_ω by

$$\begin{cases} (\Delta_x + \omega^2)G_\omega(x, y) = -\delta_y(x) & \text{in } \Omega \ (y \in \Omega), \\ \frac{\partial G_\omega}{\partial \nu_x}(x, y) = 0, & x \in \Gamma_i, \\ G_\omega(x, y) = 0, & x \in \Gamma_e. \end{cases} \quad (2.7)$$

Then, we have

$$G_\omega(x, y) = G_\omega(y, x) \quad \text{for } x \neq y \in \Omega, \quad (2.8)$$

and the solution u_0 to (2.6) is given by

$$u_0(x) = - \int_{\Gamma_e} \frac{\partial G_\omega}{\partial \nu_z}(z, x) \Phi_\omega(z - y) d\sigma(z), \quad x \in \Omega, y \in \Gamma_e, \quad (2.9)$$

which can be proved using Green's theorem.

Throughout this paper, we will denote by $\mathcal{S}_{\Gamma_i}^\omega$ the single layer potential on Γ_i associated with G_ω , that is,

$$\mathcal{S}_{\Gamma_i}^\omega[\varphi](x) = \int_{\Gamma_i} G_\omega(x, y) \varphi(y) d\sigma(y), \quad x \in \mathbb{R}^2 \quad (2.10)$$

for $\varphi \in L^2(\Gamma_i)$.

3 Asymptotic formula

We derive in this section an asymptotic expansion of the ultrasound boundary perturbations due to the presence of the corrosive parts.

Let u_γ and u_0 be the solutions to (2.5) and (2.6), respectively. Let $v := u_\gamma - u_0$. Then v satisfies

$$\begin{cases} \Delta v + \omega^2 v = 0 & \text{in } \Omega, \\ \frac{\partial v}{\partial \nu} + \gamma v = -\gamma u_0 & \text{on } \Gamma_i, \\ v = 0 & \text{on } \Gamma_e. \end{cases} \quad (3.1)$$

By integrating the first equation in (3.1) against $G_\omega(x, y)$ and using the divergence theorem, we get

$$v + \mathcal{S}_{\Gamma_i}^\omega[\gamma v] = -\mathcal{S}_{\Gamma_i}^\omega[\gamma u_0] \quad \text{in } \Omega, \quad (3.2)$$

and hence

$$\gamma v + \gamma \mathcal{S}_{\Gamma_i}^\omega[\gamma v] = -\gamma \mathcal{S}_{\Gamma_i}^\omega[\gamma u_0] \quad \text{in } \Omega. \quad (3.3)$$

The following lemma is of use to us.

Lemma 3.1 *If ϵ is sufficiently small, then the operator $I + \gamma \mathcal{S}_{\Gamma_i}^\omega$ is invertible on $L^2(\Gamma_i)$.*

Proof. Since $\gamma \mathcal{S}_{\Gamma_i}^\omega$ is a compact operator on $L^2(\Gamma_i)$, it suffices to show the injectivity of $I + \gamma \mathcal{S}_{\Gamma_i}^\omega$ by the Fredholm alternative. Suppose that $(I + \gamma \mathcal{S}_{\Gamma_i}^\omega)v = 0$ for some $v \in L^2(\Gamma_i)$. Then, it follows from (2.3) that

$$\begin{aligned} \|v\|_{L^2(\Gamma_i)} &= \|\gamma \mathcal{S}_{\Gamma_i}^\omega[v]\|_{L^2(\Gamma_i)} \\ &\leq \|\gamma\|_{L^2(\Gamma_i)} \|\mathcal{S}_{\Gamma_i}^\omega[v]\|_{L^\infty(\Gamma_i)} \\ &\leq C\epsilon^{1/2} \|v\|_{L^2(\Gamma_i)}, \end{aligned}$$

and hence $v = 0$ if ϵ is sufficiently small. This completes the proof. \square

We now derive an asymptotic formula for $\frac{\partial(u_\gamma - u_0)}{\partial \nu}$ as $\epsilon \rightarrow 0$, which will be an essential ingredient for designing the reconstruction scheme.

Theorem 3.2 *Suppose that each curve I_s is centered around a fixed point z_s . Then the following asymptotic formula holds uniformly on Γ_e as $\epsilon \rightarrow 0$:*

$$\frac{\partial(u_\gamma - u_0)}{\partial\nu}(x) = -\sum_{s=1}^m \langle \gamma \rangle_s u_0(z_s) \frac{\partial G_\omega}{\partial\nu}(x, z_s) + O(\epsilon^{1+\frac{1}{p}}), \quad x \in \Gamma_e, \quad (3.4)$$

for all $p > 1$, where

$$\langle \gamma \rangle_s := \int_{I_s} \gamma(x) d\sigma(x).$$

Proof. Since there exists a positive constant C depending only on p, ω , and r such that for $p > 1$

$$\|\mathcal{S}_{\Gamma_i}^\omega[\gamma v]\|_{L^\infty(\Gamma_i)} \leq C \|\gamma v\|_{L^p(\Gamma_i)} \leq C \epsilon^{\frac{1}{p}} \|v\|_{L^\infty(\Gamma_i)}$$

and

$$\|\mathcal{S}_{\Gamma_i}^\omega[\gamma u_0]\|_{L^\infty(\Gamma_i)} \leq C \epsilon^{\frac{1}{p}} \|u_0\|_{L^\infty(\Gamma_i)},$$

it follows from (3.2) that

$$\|v\|_{L^\infty(\Gamma_i)} \leq C \epsilon^{\frac{1}{p}} \quad (3.5)$$

for some constant $C = C(p, \omega, r, R)$. Since the distance between Γ_e and Γ_i is $R - r$, we get from (3.2) that

$$\left\| \frac{\partial}{\partial\nu} \mathcal{S}_{\Gamma_i}^\omega[\gamma v] \right\|_{L^\infty(\Gamma_e)} \leq C \|\gamma v\|_{L^1(\Gamma_i)} \leq C \|\gamma\|_{L^1(\Gamma_i)} \|v\|_{L^\infty(\Gamma_i)} \leq C \epsilon^{1+\frac{1}{p}}, \quad (3.6)$$

where C depends on p, ω, r , and R . We now obtain from (3.2) and (3.6) that

$$\frac{\partial v}{\partial\nu}(x) = -\int_{\Gamma_i} (\gamma u_0)(y) \frac{\partial G_\omega}{\partial\nu(x)}(x, y) d\sigma(y) + O(\epsilon^{1+\frac{1}{p}}) \quad \text{in } L^\infty(\Gamma_e). \quad (3.7)$$

Since

$$\frac{\partial G_\omega}{\partial\nu}(x, y) = \frac{\partial G_\omega}{\partial\nu}(x, z_s) + O(|y - z_s|), \quad y \in I_s$$

and

$$\int_{\Gamma_i} \gamma u_0 d\sigma = \sum_s \langle \gamma \rangle_s u_0(z_s) + O(\epsilon^2 \|\nabla u_0\|_{L^\infty(\Gamma_i)}),$$

we obtain the desired result (3.4). \square

We shall make two remarks on the asymptotic formula (3.4). Theorem 3.2 justifies a Born approach to the problem. Ignoring the term γv in (3.1), we have

$$v(x) \approx -\sum_{s=1}^m \langle \gamma \rangle_s u_0(z_s) G_\omega(x, z_s)$$

for x away from Γ_i , which yields (3.4).

On the other hand, formula (3.4) is valid when ω is fixed and ϵ goes to zero. But its frequency dependency is not clear in its present form. Finding precisely this frequency dependency is a very challenging problem because of the multiple scattering configuration. In this direction we perform some numerical experiments in the next section.

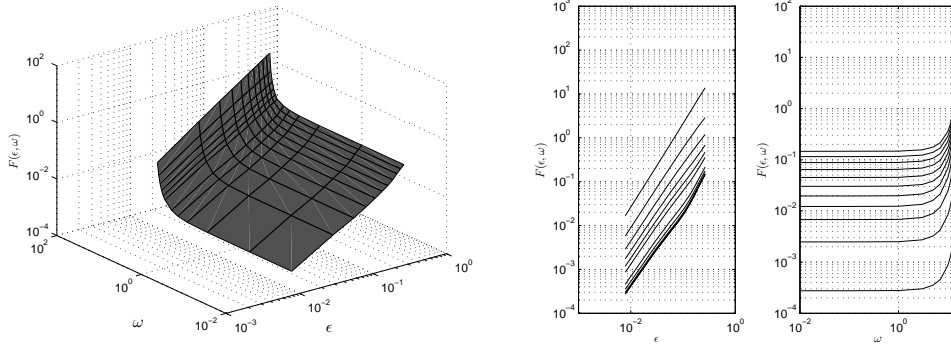


Figure 2: All the graphs are in log-log scale. The figure on the left is the graph of $F(\epsilon, \omega)$. The first one on the right is the graph of $F(\epsilon, \omega)$ for various ϵ , but fixed ω . They are straight lines of slope 2. The second one on the right is $F(\epsilon, \omega)$ for various ω , but fixed ϵ .

4 High-frequency asymptotic formula-numerical experiment

In order to investigate the frequency dependency of (3.4), we compute numerically

$$F(\epsilon, \omega) := \left\| \frac{\partial(u_\gamma - u_0)}{\partial\nu}(x) + \sum_{s=1}^m \langle \gamma \rangle_s u_0(z_s) \frac{\partial G_\omega}{\partial\nu}(x, z_s) \right\|_{L^\infty(\Gamma_e)} \quad (4.1)$$

for various ϵ and ω .

For computations we take the domain $\Omega \subset \mathbb{R}^2$ to be the annulus centered at $(0,0)$ with radii 0.5 and 0.4. The corrosive part I consists of a single arc with the corrosion coefficient $\gamma = 2$. We choose the mesh points $N = 960$ on each of Γ_e and Γ_i . The number N is enough to resolve the highest frequency ($\omega = 15$). We then compute the values of $F(\epsilon, \omega)$ for various ϵ and ω : $\omega = 0.01, 0.1, 1, 3, \dots, 15$ and $0.0079 \leq \epsilon \leq 0.2644$. Figure 2 shows the results. The first figure on the right clearly shows that the dependency on ϵ is ϵ^2 . The second one tells us that the dependency on ω is much more subtle because of the multiple scattering configuration: something of the form $e^{\psi(\omega)}$ for some function $\psi(\omega)$, which is almost constant for low values of ω (low frequencies) and rapidly increasing for high values of ω . The threshold is about 7. The wavelength $2\pi/\omega$ is about 10 times the distance between Γ_i and Γ_e . The exponential behavior seems to be the result of a Neumann series in ω^2 of the wave generated by the corrosive part.

These computations suggest that the following formula holds:

$$\frac{\partial(u_\gamma - u_0)}{\partial\nu}(x) = - \sum_{s=1}^m \langle \gamma \rangle_s u_0(z_s) |I_s| \frac{\partial G_\omega}{\partial\nu}(x, z_s) + O(\epsilon^2 e^{\psi(\omega)}), \quad x \in \Gamma_e. \quad (4.2)$$

5 Reconstruction methods

In this section, we adapt the MUSIC-type algorithm of [7] to the setting in which multiple ultrasound boundary measurements are available and also show how one may quantitatively deduce the number of corrosive parts present. Our approach relies on the asymptotic expansion (3.4) of the ultrasound reflected wave with respect to the length of the corrosive parts.

5.1 A MUSIC-type algorithm

Let us first introduce the notion of the Dirichlet-to-Neumann (DtN) map. Let u_γ be the solution to the problem (2.5) and define the DtN map Λ_γ^ω by

$$\Lambda_\gamma^\omega[y] := \frac{\partial u_\gamma}{\partial \nu} \Big|_{\Gamma_e}. \quad (5.1)$$

Let Λ_0^ω be the DtN map when there is no corrosion. We also define T^ω by

$$T^\omega[y](x) = - \sum_{s=1}^m \langle \gamma \rangle_s u_0(z_s) \frac{\partial G_\omega}{\partial \nu}(x, z_s), \quad x \in \Gamma_e. \quad (5.2)$$

Observe that the dependency of $T^\omega[y]$ on y is hidden in the term $u_0(z_s)$ where u_0 is the solution to (2.6). Then the formula (3.4) now reads

$$(\Lambda_\gamma^\omega - \Lambda_0^\omega)[y] \approx T^\omega[y]. \quad (5.3)$$

The MUSIC algorithm of this paper is based on the following simple observation.

Lemma 5.1 *Suppose that ω is not a Dirichlet eigenvalue of $-\Delta$ in the disk of radius R . Let Φ_ω and G_ω be the functions defined by (2.4) and (2.7), respectively. For $z \in \Gamma_i$ and $x \in \Gamma_e$, let the indicator function*

$$h_z(x) := \int_{\Gamma_e} \frac{\partial G_\omega}{\partial \nu}(y, z) \Phi_\omega(y - x) d\sigma(y). \quad (5.4)$$

If there are complex numbers a_1, \dots, a_m such that

$$h_z(x) = \sum_{s=1}^m a_s h_{z_s}(x) \quad \text{for all } x \in \Gamma_e, \quad (5.5)$$

then $z \in \{z_1, \dots, z_m\}$.

Proof. We first observe that if ω is not a Dirichlet eigenvalue of $-\Delta$ in the disk of radius R and $\int_{\Gamma_e} f(y) \Phi_\omega(y - x) d\sigma(y) = 0$ for all $x \in \Gamma_e$, then $f \equiv 0$, a proof of which can be found in [11]. The relation (5.5) implies that

$$\int_{\Gamma_e} \left[\frac{\partial G_\omega}{\partial \nu}(y, z) - \sum_{s=1}^m a_s \frac{\partial G_\omega}{\partial \nu}(y, z_s) \right] \Phi_\omega(y - x) d\sigma(y) = 0 \quad \text{for all } x \in \Gamma_e,$$

from which it follows that

$$\frac{\partial G_\omega}{\partial \nu}(y, z) - \sum_{s=1}^m a_s \frac{\partial G_\omega}{\partial \nu}(y, z_s) = 0 \quad \text{for all } y \in \Gamma_e. \quad (5.6)$$

Since $G_\omega(y, z) = \sum_{s=1}^m a_s G_\omega(y, z_s) = 0$ for all $y \in \Gamma_e$, we have from (5.6) and the unique continuation that $G_\omega(y, z) = \sum_{s=1}^m a_s G_\omega(y, z_s)$ for all $y \in \Omega$. Since $G_\omega(y, z)$ has singularity at $y = z$ while $\sum_{s=1}^m a_s G_\omega(y, z_s)$ has at $y = z_s$ for those s such that $a_s \neq 0$, we conclude that $z = z_s$ for some s . This completes the proof. \square

We now discretize the relation (5.5) using uniformly spaced set $\{y_1, \dots, y_N\}$ on Γ_e for a sufficiently large N to conclude that if there are complex numbers a_1, \dots, a_m such that

$$h_z(y_\ell) = \sum_{s=1}^m a_s h_{z_s}(y_\ell) \quad \text{for } \ell = 1, \dots, N, \quad (5.7)$$

then z approximately equals to z_s for some $s = 1, \dots, m$. This is the MUSIC characterization of the location of corrosive parts z_s . Let us put, for $z \in \Gamma_i$,

$$h_z := (h_z(y_1), \dots, h_z(y_N))^T.$$

Then the condition (5.7) is equivalent to

$$h_z \text{ is a linear combination of } \{h_{z_1}, \dots, h_{z_m}\}. \quad (5.8)$$

Thus the main task in determining the location of corrosive parts is to determine those z which satisfy the condition (5.8).

It should be emphasized that we do not have those vectors h_{z_s} in our hand since we do not know the location z_s of the corrosive parts. The key fact in designing the algorithm is that even if we do not know the individual h_{z_s} , the space spanned by h_{z_s} , $s = 1, \dots, m$, can be characterized by the boundary measurements, and hence the condition (5.8) can be checked. Let u_0^ℓ be the solutions to (2.6) with $y = y_\ell$, for $\ell = 1, \dots, N$. Since

$$u_0^\ell(z_s) = - \int_{\Gamma_e} \frac{\partial G_\omega}{\partial \nu}(y, z_s) \Phi_\omega(y - y_\ell) d\sigma(y) = -h_{z_s}(y_\ell),$$

we have

$$T^\omega[y_\ell](y) = \sum_{s=1}^m \langle \gamma \rangle_s h_{z_s}(y_\ell) \frac{\partial G_\omega}{\partial \nu}(y, z_s). \quad (5.9)$$

In the spirit of the reciprocity gap approach [9, 8], multiplying by $\Phi_\omega(y - y_{\ell'})$ and integrating over Γ_e , we obtain

$$\int_{\Gamma_e} T^\omega[y_\ell](y) \Phi_\omega(y - y_{\ell'}) d\sigma(y) = \sum_{s=1}^m \langle \gamma \rangle_s h_{z_s}(y_\ell) h_{z_s}(y_{\ell'}). \quad (5.10)$$

Define $T_N = (t_{\ell\ell'})_{\ell, \ell'=1}^N$ by

$$t_{\ell\ell'} = \int_{\Gamma_e} T^\omega[y_\ell](y) \Phi_\omega(y - y_{\ell'}) d\sigma(y).$$

Then (5.10) shows that the condition (5.8) is equivalent to

$$h_z \in \text{Range}(T_N). \quad (5.11)$$

Define $N \times N$ matrix Λ_N by

$$\Lambda_N = \left(\int_{\Gamma_e} (\Lambda_\gamma^\omega - \Lambda_0^\omega)[y_\ell](y) \Phi_\omega(y - y_{\ell'}) d\sigma(y) \right)_{\ell, \ell'=1}^N. \quad (5.12)$$

According to (5.3), we have

$$\Lambda_N \approx T_N = \left(\sum_{s=1}^m \langle \gamma \rangle_s h_{z_s}(y_\ell) h_{z_s}(y_{\ell'}) \right)_{l, l'}, \quad (5.13)$$

and hence in view of (5.11) the algorithm is to determine those $z \in \Gamma_i$ satisfying

$$h_z \in \text{Range}(\Lambda_N). \quad (5.14)$$

The function $z \mapsto h_z$ is an indicator function. We interpret the points z where the vectors h_z are in the range of the matrix Λ_N as good candidates for the z_s . Note that Λ_N is computed using the boundary measurements $(\Lambda_\gamma^\omega - \Lambda_0^\omega)[y_\ell]$. Note also that since $\Lambda_\gamma^\omega - \Lambda_0^\omega$ is self-adjoint in the sense that

$$\int_{\Gamma_e} (\Lambda_\gamma^\omega - \Lambda_0^\omega)[x](y) \Phi_\omega(y - z) d\sigma(y) = \int_{\Gamma_e} (\Lambda_\gamma^\omega - \Lambda_0^\omega)[z](y) \Phi_\omega(y - x) d\sigma(y)$$

for all $x, z \in \Gamma_e$, which can be proved easily, Λ_N is symmetric and hence admits a (orthogonal) singular value decomposition (SVD). Using eigenvectors of Λ_N we can characterize those z satisfying (5.14).

Let us summarize the algorithm which generalizes the one in [7].

[MUSIC-type Algorithm]

- Step 1.** Obtain the Neumann data $(\Lambda_\gamma^\omega - \Lambda_0^\omega)(y_\ell)$ on Γ_e for $y_\ell \in \Gamma_e$, $\ell = 1, \dots, N$;
- Step 2.** Compute the matrix Λ_N ;
- Step 3.** Compute the SVD of Λ_N . Let $\lambda_1 \geq \lambda_2 \geq \dots$ be the eigenvalues of Λ_N and let $\{v_p, p = 1, 2, \dots\}$ be an orthonormal basis of eigenfunctions;
- Step 4.** For $k = 1, 2, \dots$, let P_k be the orthogonal projector on to the space spanned by $\{v_1, \dots, v_k\}$ and define $\theta_k(z)$ by

$$\cot \theta_k(z) = L_k := \frac{\|P_k(h_z)\|}{\|(I - P_k)(h_z)\|}. \quad (5.15)$$

We then compute the minimal values of $\theta_k(z)$ using k eigenvectors. We start this process with just one singular vector ($k = 1$) and continue with increasing k until the plot of $\theta_k(z)$ stabilizes. Values near zero correspond to locations are that likely to be close to the corrosive parts I_s (or z_s).

- Step 5.** We then determine approximately the corrosion coefficients $\langle \gamma \rangle_s$ by solving the linear system (5.13).

It is worth emphasizing that in (5.12), l and l' may respectively vary from 1 to N and 1 to N' , with $N \neq N'$. In that case the response matrix Λ_N is not a square matrix but still admits an SVD. As shown in the numerical examples, N may be much smaller than N' .

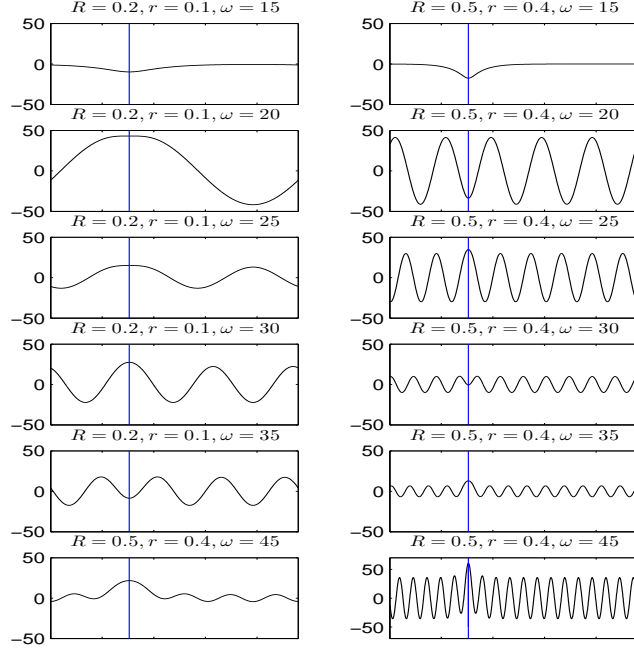


Figure 3: Oscillations of $\frac{\partial G}{\partial \nu_x}(x, z)$ on $x \in \Gamma_e$ for various ω and fixed $z \in \Gamma_i$. The blue dotted line indicates the location of z .

6 High-frequency instabilities

In many practical situations, $R - r$ is of order r and much larger than the wavelength $\lambda = 2\pi/\omega$ while ϵ is much smaller than λ . In this case, formula (4.2) remains valid but does not yield a stable detection procedure because of high oscillations in the computations of $\frac{\partial G_\omega}{\partial \nu}$ and h_z defined by (5.4). In fact, Figure 3 shows the oscillations of $\frac{\partial G_\omega}{\partial \nu_x}(\cdot, z)$ on Γ_e for $\omega = 10, 18, 20, 30, 40, 50$, and Figure 4 shows those of h_z for $\omega = 1, 10, 15, 18, 20$.

To resolve this difficulty, we first introduce the truncation operator \mathcal{P}_n defined by

$$\mathcal{P}_n(f) := \sum_{|\ell| \leq n} f_\ell e^{i\ell\theta} \quad (6.1)$$

for $n = 1, 2, \dots$, when f is given in its Fourier series by $f = \sum_{\ell \in \mathbb{Z}} f_\ell e^{i\ell\theta}$. The operator \mathcal{P}_n is a low pass filter operator. We choose $n = \omega(R - r)$ as the threshold of the truncation.

To justify the validity of this filtering, consider the Helmholtz equation $(\Delta + \omega^2)w = 0$ in $|x| > r$ with the boundary condition $w = f$ on $|x| = r$. Then we have

$$w(R, \theta) = \sum_{l \in \mathbb{Z}} f_l \frac{H_l^{(1)}(\omega R)}{H_l^{(1)}(\omega r)} e^{il\theta}, \quad R > r.$$

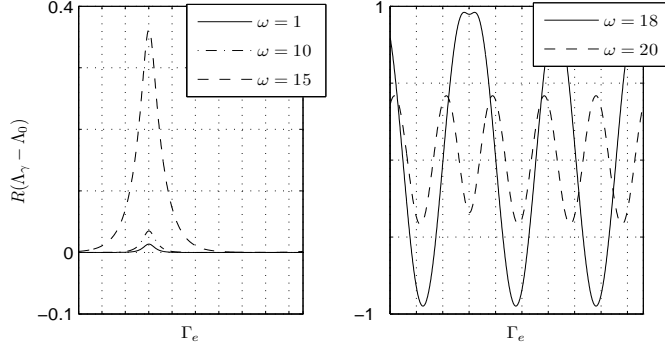


Figure 4: Oscillations of $\frac{\partial(u_\epsilon - u_0)}{\partial\nu}$ for various ω when $\epsilon = 7.8540e - 3$.

By making use of Debey's asymptotic expansion [1, page 366] (see also [16]),

$$\frac{H_l^{(1)}(\omega R)}{H_l^{(1)}(\omega r)} \approx \frac{e^{l(\alpha - \tanh \alpha)}}{e^{l(\alpha' - \tanh \alpha')}}, \quad \text{for } l > \omega R, \quad (6.2)$$

where $\omega R = l \operatorname{sech} \alpha$ and $\omega r = l \operatorname{sech} \alpha'$. Note that $\alpha' > \alpha$. Moreover, from the asymptotic behavior of Hankel functions [1, 9.3.3], *i.e.*,

$$H_l^{(1)}(l \sec \beta) = \sqrt{2/(\pi l \tan \beta)} \{e^{i(l \tan \beta - l\beta - \frac{1}{4}\pi)} + O(l^{-1})\}, \quad 0 < \beta < \frac{1}{2}\pi,$$

we have

$$\frac{H_l^{(1)}(\omega R)}{H_l^{(1)}(\omega r)} \approx \sqrt{\frac{\tan \beta'}{\tan \beta}} e^{i(l \tan \beta - l\beta - l \tan \beta' + l\beta')} \quad \text{for } l < \omega r, \quad (6.3)$$

where $\omega R = l \sec \beta$ and $\omega r = l \sec \beta'$.

From (6.2) we see that the Helmholtz operator acts as a low pass filter. It filters all the f_l for l larger than ωr . Moreover, in the case where $R - r$ is of order r and $r \gg \lambda := 2\pi/\omega$, (6.3) would suggest that the angular resolution is of order $\pi/\omega r = \lambda/(2r)$. This means that if the distance between two corrosive parts is less than $\lambda/2$, then they cannot be detected separately.

Now it follows from (4.2) that

$$\mathcal{P}_n \left[\frac{\partial(u_\gamma - u_0)}{\partial\nu} \right] \approx - \sum_{s=1}^m \gamma(z_s) u_0(z_s) |I_s| \mathcal{P}_n \left[\frac{\partial G_\omega}{\partial\nu} \right] (\cdot, z_s) \quad \text{on } \Gamma_e,$$

since \mathcal{P}_n is linear. The necessary modifications of our MUSIC procedure are obvious. They simply consist in filtering high-frequency oscillations in the function h_z defined by (5.4). We should replace h_z by

$$h_z(x) := \mathcal{P}_n \left(\int_{\Gamma_e} \mathcal{P}_n \left[\frac{\partial G_\omega}{\partial\nu} \right] (y, z) \Phi_\omega(y - x) d\sigma(y) \right). \quad (6.4)$$

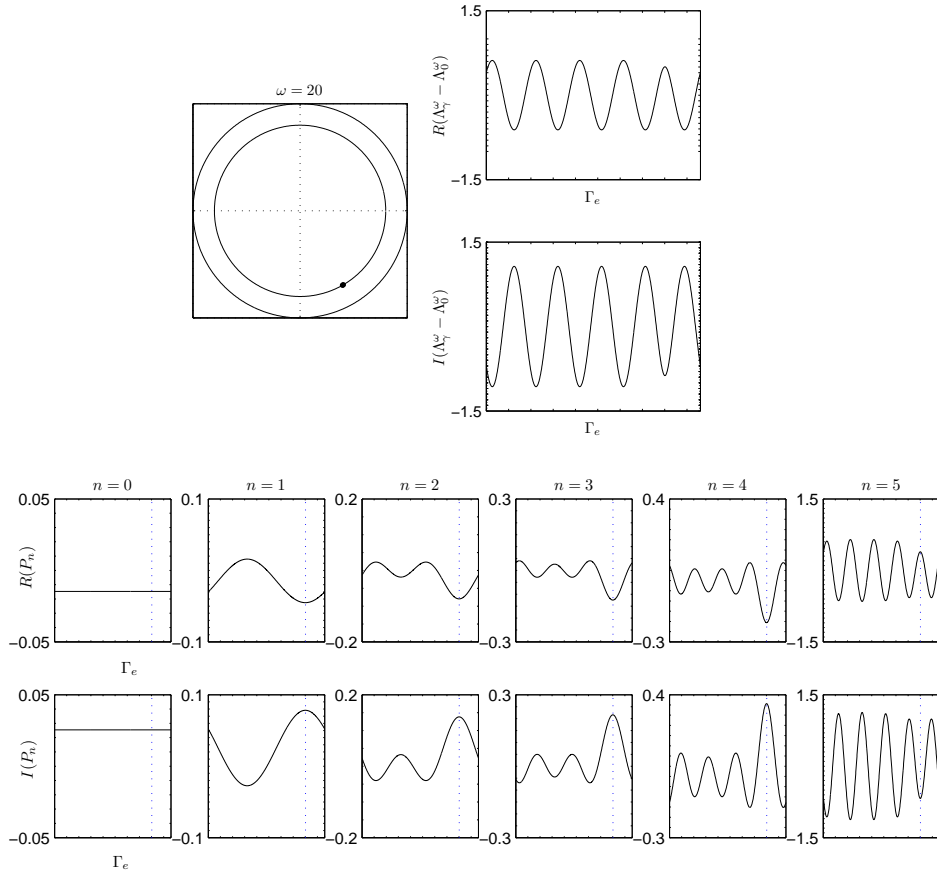
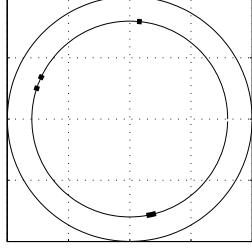


Figure 5: Top-left is the actual configuration of the corrosive pipe. The operating frequency $\omega = 20$. Top-right are the real and imaginary parts of the measurements without using filtering. The two bottom rows are filtered measurements $\mathcal{P}_n(\Lambda_\gamma^\omega - \Lambda_0^\omega)$ for various n . The data without filtering does not yield much information on the location of the corrosive part. But the filtered data with $n = 2, 3, 4$ yield enough information to determine the location. Here the threshold $\omega(R - r) = 2$.

Figure 5 shows the projected measurements $\mathcal{P}_n \left[\frac{\partial(u_\gamma - u_0)}{\partial\nu} \right]$ for various n at $\omega = 20$. The measurement $\frac{\partial(u_\gamma - u_0)}{\partial\nu}$ does not seem to yield any useful information on the location of the corrosive part. But the filtering, especially for $n = 2, 3, 4$, clearly exhibits the location z .

7 Numerical results

This section presents numerical results of finding the internal corrosive parts, using the MUSIC-type algorithm. In the following, $\Omega \subset \mathbb{R}^2$ is assumed to be the annulus centered at



m	ω	γ_s	z_s	$\langle \gamma \rangle_s$	I_s
4	5	2	(7.8414e-2, 7.9615e-1)	1.1781e-1	5.8905e-2
		0.05	(-7.2319e-1, 3.4204e-1)	2.9452e-3	5.8905e-2
		0.1	(-7.5962e-1, 2.5095e-1)	5.8905e-3	5.8905e-2
		1	(1.7528e-1, -7.8056e-1)	9.8175e-2	9.8175e-2

Figure 6: The actual pipe with four corrosive parts.

$(0, 0)$ with radii, R and r . Γ_e and Γ_i are the outer and inner boundaries of Ω , respectively. Let $I_s, s = 1, \dots, m$, be the corrosive parts with the corrosion coefficient γ_s .

For the computations, we discretize Γ_e by $\{y_1, \dots, y_N\}$, where

$$y_n := r_e (\cos(\theta_n + \pi/N), \sin(\theta_n + \pi/N)) \quad \text{and} \quad x_n := r_i (\cos \theta_n, \sin \theta_n)$$

with $\theta_n = 2\pi(n-1)/N$ for $n = 1, \dots, N$. Here we take $N = 256$.

In order to obtain the measurements $(\Lambda_\gamma^\omega - \Lambda_0^\omega)[y_n]$ on Γ_e for $n = 1, \dots, N$, we solve the direct problems (2.5) and (2.6) using the boundary integral method based on the layer potentials for the Helmholtz equation. For doing this, there is one technical difficulty. If we use the same discrete points $\{y_n\}$ to evaluate $(\Lambda_\gamma^\omega - \Lambda_0^\omega)[y_n](y_m)$ numerically, then $(\Lambda_\gamma^\omega - \Lambda_0^\omega)[y_n](y_m)$ blows up if $n = m$. To avoid this technical difficulty, we evaluate $(\Lambda_\gamma^\omega - \Lambda_0^\omega)[y_n]$ at points $\tilde{y}_m = r_e (\cos \theta_n, \sin \theta_n)$ for $m = 1, \dots, N$. In other words the response matrix $((\Lambda_\gamma^\omega - \Lambda_0^\omega)[y_n](\tilde{y}_m))_{n,m=1}^N$ is our measurements.

In the following examples, the outer radius $R = 1$ and the inner one $r = 0.8$ and there are four corrosive parts. Figure 6 shows the actual domain with corrosive parts.

Using the response matrix $((\Lambda_\gamma^\omega - \Lambda_0^\omega)[y_n](\tilde{y}_m))_{n,m=1}^N$, we compute the matrix Λ_N defined by (5.12). In doing this we add $p\%$ random noise to the measurements for $p = 0, 1, 5, 10$. Adding $p\%$ noise means that our measurement becomes

$$w + \frac{p}{100} \text{rand}(1) \max\{|w|\},$$

where w is the actual measurement (the computed response matrix) on Γ_e . Here $\text{rand}(1)$ is a random number generator in $(-1, 1)$.

Figure 7 shows the computed Λ_N under various noise levels. It should be noted that we set the frequency $\omega = 5$.

Figure 8 shows the computational results of the MUSIC-type algorithm. The top figures are SVDs of Λ_N and T_N . The SVD of T_N exhibits a clear drop of the eigenvalues after four significant eigenvalues, which is the number of the corrosive parts. On the other hand, the SVD of Λ_N shows a larger number of significant eigenvalues, which corresponds to the number of nodal points of Γ_i inside the corrosive parts. The figures in the middle are the graphs of θ_k defined by (5.15) for $k = 1, 2, \dots$, where k denotes the number of eigenvectors of Λ_N used. We can see that the second and third corrosive parts are detected when there is no noise (see (c) of Figure 8). When there is noise, it is interesting to note that since the

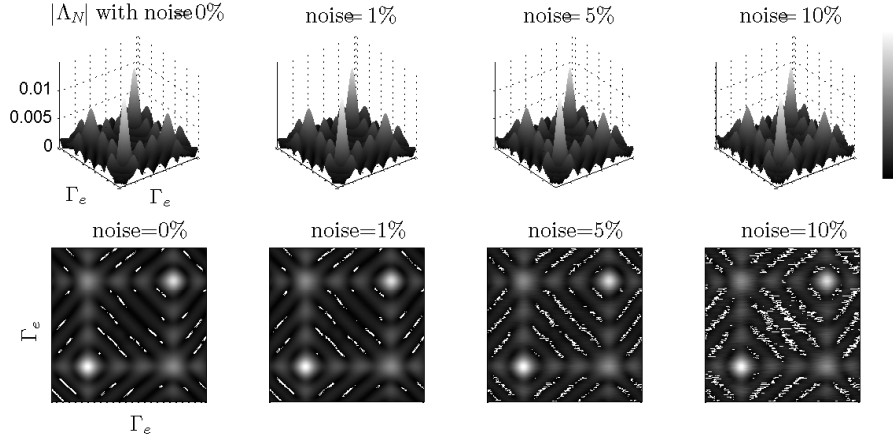


Figure 7: Λ_N under various noise level. The bottom figures are projections.

noise(%)	m^c	z_s^c	$\langle \gamma \rangle_s^c$	$ z_s - z_s^c $	$ \langle \gamma \rangle_s - \langle \gamma \rangle_s^c $
0	4	(7.8414e-2, 7.9615e-1)	1.0435e-1	0.0000e0	1.3492e-2
		(-7.2319e-1, 3.4204e-1)	3.0301e-3	0.0000e0	8.4898e-5
		(-7.5962e-1, 2.5095e-1)	5.7961e-3	0.0000e0	9.4447e-5
		(1.7528e-1,-7.8056e-1)	8.9050e-2	0.0000e0	9.1335e-3
1	3	(7.8414e-2, 7.9615e-1)	1.0438e-1	0.0000e0	1.3460e-2
		(-7.4639e-1, 2.8792e-1)	8.4656e-3	3.9266e-2	2.5751e-3
		(1.7528e-1,-7.8056e-1)	8.9065e-2	0.0000e0	9.1205e-3
5	3	(7.8414e-2, 7.9615e-1)	1.0438e-1	0.0000e0	1.3464e-2
		(-7.4639e-1, 2.8792e-1)	8.3812e-3	3.9266e-2	2.4918e-3
		(1.7528e-1,-7.8056e-1)	8.9092e-2	0.0000e0	9.0995e-3
10	3	(7.8414e-2, 7.9615e-1)	1.0433e-1	0.0000e0	1.3518e-2
		(-7.5324e-1, 2.6951e-001)	8.2734e-3	1.9634e-2	2.3859e-3
		(1.7528e-1,-7.8056e-1)	8.9137e-2	0.0000e0	9.0642e-3

Table 1: The computational results of the MUSIC-type algorithm with $\omega = 5$.

second and third corrosive parts are close to each other and have relatively low coefficients, they are detected as a single one. Table 1 shows the numerical values of detected quantities. The corrosion coefficients are computed by solving the linear system (5.13).

Since the number of significant eigenvalues of the response matrix Λ_N contains information not only on the number of corrosive parts but also on the number of nodal points, as was already observed in [7, 6], we are able to identify the length of the corrosive part. Figure 9 is for the detection of a corrosive part of length of order the wavelength $2\pi/\omega$. The used frequency is $\omega = 5$ and the number of used eigenvectors is $k = 20$. Values of θ_k near zero correspond to the location of the corrosive part. Figure 9 shows that the algorithm of this paper works well for detecting corrosion of size comparable to the wavelength and the length of the corrosive parts can be accurately reconstructed.

Figure 10 shows the performance of the MUSIC-type algorithms at frequencies $\omega = 1, 5, 50, 100$. It clearly exhibits the high-frequency instability. We emphasize that for this computation and the next one we use the discretization $N = 960$ (to enhance the precision of the computation) and the number of source points 10 (to reduce the computation time). So Λ_N here is 10×960 matrix, not 256×256 . The corrosion coefficient is set to be $\gamma = 0.05$.

We then compare these results with those when we use the filtering. The filtering operator \mathcal{P}_n is defined, as before, by

$$\mathcal{P}_n[f] := \sum_{|\ell| \leq \omega(r_e - r_i)} f_\ell e^{i\ell\theta},$$

where f_ℓ is the Fourier coefficients of f . Figure 11 shows the comparison. It clearly illustrates that by filtering we are able to overcome the high-frequency instability.

8 Conclusion

In this paper we have developed a non-iterative algorithm for locating small internal corrosive parts in pipelines from exterior ultrasound boundary measurements. Our algorithm is based on an asymptotic expansion of the effect of the corrosion in terms of the size of the corrosive parts. We have numerically tested the validity of such an asymptotic formula at high-frequencies. We have also proposed a simple procedure to remove high-frequency instabilities in our inversion procedure in the case where the wavelength is small compared to the distance between the accessible and inaccessible parts of the pipeline. Finally, we have presented many computational experiments to show the robustness and the accuracy of our detection algorithm.

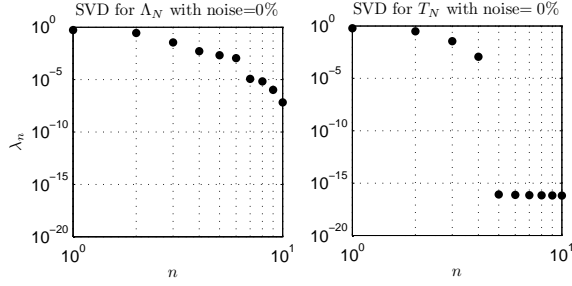
Acknowledgements

The authors are very grateful to the reviewers for their comments and suggestions to improve the presentation of the paper.

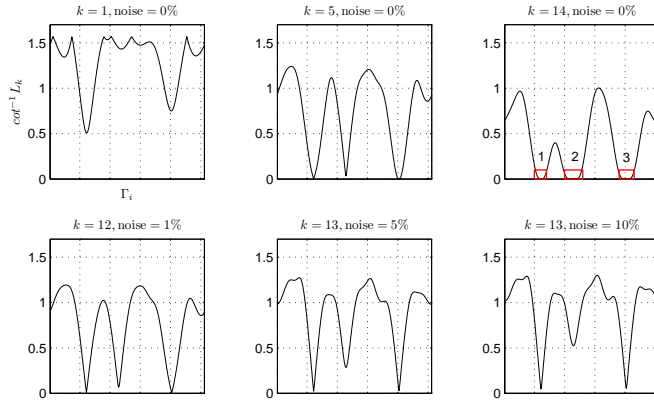
References

- [1] M. Abramowitz and I. Stegun (editors), *Handbook of Mathematical Functions*, National Bureau of Standards, Washington D.C., 1964.
- [2] P.M. Anselone, *Collectively Compact Operator Approximation Theory and Applications to Integral Equations*, Prentice-Hall, Englewood Cliffs, 1971.
- [3] H. Ammari, E. Iakovleva, and D. Lesselier, A MUSIC algorithm for locating small inclusions buried in a half-space from the scattering amplitude at a fixed frequency, *SIAM Multiscale Model. Simul.*, 3 (2005), 597–628.
- [4] H. Ammari, H. Kang, and E. Kim, Detection of internal corrosion, *ESAIM: Proc.*, 26 (2009), 207–216.
- [5] H. Ammari, H. Kang, E. Kim, H. Lee, and K. Louati, Vibration testing for detecting internal corrosion, *Stud. Appl. Math.*, 122 (2009), 85–104.

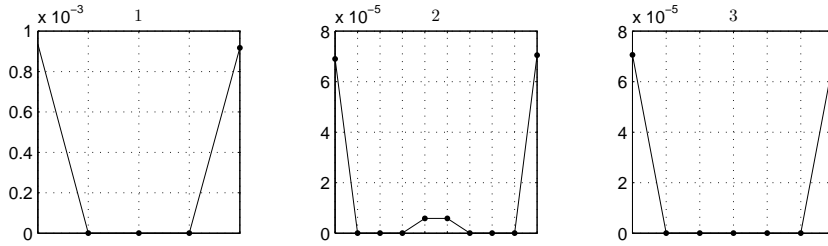
- [6] H. Ammari, H. Kang, H. Lee, and W.K. Park, Asymptotic imaging of perfectly conducting cracks, *SIAM J. Sci. Comp.*, 32 (2010), 894–922.
- [7] H. Ammari, H. Kang, E. Kim, K. Louati, and M. Vogelius, A MUSIC-type algorithm for detecting internal corrosion from steady state voltage boundary perturbations, *Numer. Math.*, 108 (2008), 501–528.
- [8] H. Ammari, S. Moskow, and M. Vogelius, Boundary integral formulae for the reconstruction of electric and electromagnetic inhomogeneities of small volume, *ESAIM: Cont. Opt. Calc. Var.* 9 (2003), 49–66.
- [9] S. Andrieux and A. Ben Abda, Identification de fissures planes par une donnée de bord unique; un procédé direct de localisation et d’identification, *C. R. Acad. Sci., Paris I* 315 (1992), 1323–1328.
- [10] M. Cheney, The linear sampling method and the MUSIC algorithm, *Inverse Problems*, 17 (2001), 591–595.
- [11] D. Colton and R. Kress, *Inverse Acoustic and Electromagnetic Scattering Theory*, 2nd ed. Berlin, Germany: Springer-Verlag, 1998.
- [12] A. J. Devaney, Time reversal imaging of obscured targets from multistatic data, *IEEE Trans. Antennas Propagat.*, 523 (2005), 1600–1610.
- [13] A. Kirsch, The MUSIC-algorithm and the factorization method in inverse scattering theory for inhomogeneous media, *Inverse Problems*, 18 (2002), 1025–1040.
- [14] F. Natterer and F. Wübbeling, *Mathematical Methods in Image Reconstruction*, SIAM Monographs on Mathematical Modeling and Computation, SIAM, Philadelphia, 2001.
- [15] F. Natterer and F. Wübbeling, Marching schemes for inverse acoustic scattering problems, *Numer. Math.*, 100 (2005), 697–710.
- [16] G.N. Watson, *A Treatise on the Theory of Bessel Functions*, Cambridge University Press, Cambridge, England, 1944.



(a) The comparison of SVD: T_N has four significant eigenvalues which correspond to the number of corrosive parts. Λ_N exhibits more than four significant eigenvalues which correspond to the number of nodal points inside the corrosive parts.



(b) The values of θ_k given by (5.15) increasing the number k of used eigenvectors under various noise levels. The horizontal axis is the curvilinear coordinate on Γ_i .



(c) Zoom of the third figure above.

Figure 8: The MUSIC-type algorithm with $\omega = 5$.

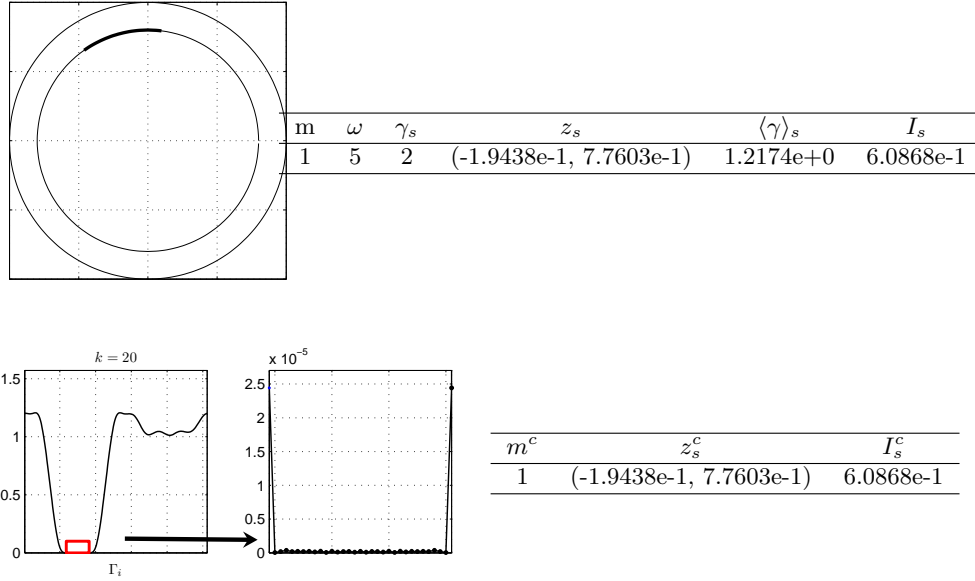


Figure 9: Imaging of an extended corrosive part under 0% noise. The length of the corrosive part can be detected.

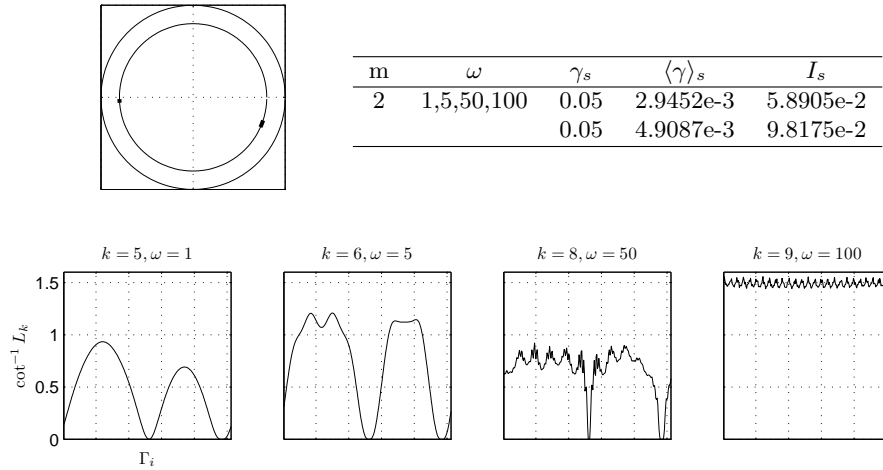


Figure 10: The MUSIC-type algorithm for various frequencies. The performance of the algorithm degrades as the frequency increases. Here k is the number of eigenvectors used.

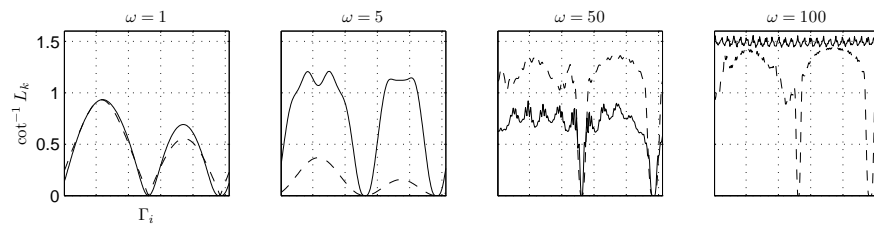


Figure 11: A comparison of MUSIC-Type algorithm with and without filtering. The solid lines are results without using the filtering and the dashed lines are results using filtering.